

A L I C E { I N T { 2 0 0 3 { 3 7  
I n t e r n a l N o t e / P H O S  
2 7 O c t o b e r 2 0 0 4

D i r e c t P h o t o n I d e n t i c a t i o n w i t h A r t i c i a l N e u r a l  
N e t w o r k i n t h e P h o t o n S p e c t r o m e t e r P H O S

M . Y u . B o g o l y u b s k y , Y u . V . K h a r l o v , S . A . S a d o v s k y  
I n s t i t u t e f o r H i g h E n e r g y P h y s i c s , P o b e d a s t r . , 1 ,  
P r o t v i n o , 1 4 2 2 8 1 , R u s s i a

A b s t r a c t

A neural network method is developed to discriminate direct photons from the neutral pion background in the PHOS spectrometer of the ALICE experiment at the LHC collider. The neural net has been trained to distinguish different classes of events by analyzing the energy-profile tensor of a cluster in its eigen vector coordinate system. Monte-Carlo simulations show that this method diminishes by an order of magnitude the probability of  $\pi^0$ -meson misidentification as a photon with respect to the direct photon identification efficiency in the energy range up to 120 GeV.

## 1 Introduction

The Large Ion Collider Experiment ALICE [1] is intended to study heavy-ion collisions at the energy of 5.5 TeV per nucleon at the LHC collider. For photons detection ALICE is equipped by the Photon Spectrometer (PHOS) [2] which is a high-granularity electromagnetic calorimeter built of lead-tungstate crystals ( $PbWO_4$ ) with the transverse dimension of  $2.2 \times 2.2 \text{ cm}^2$  and the length of 18 cm. The PHOS detector consists of  $n$  modules, each made as a matrix of  $56 \times 64$  crystals located at 460 cm from the beam interaction point. The spectrometer is positioned at the bottom of the ALICE set-up covering  $|\eta| < 0.135$  in pseudorapidity and  $100^\circ$  in the azimuthal angle.

The ALICE set-up is rather transparent to  $\gamma$ -radiation. To reach PHOS, the produced photons pass through the Inner Tracking System (ITS) [3], the Time Projection Chamber (TPC) [4] and the Charge Particle Veto Detector (CPV) [5]. The stratum of medium takes  $\sim 0.1$  of the radiation length [6] (with the main contribution from ITS and TPC), which gives a small probability of the secondary photon production in the medium.

One of the tasks of the ALICE experiment is to detect direct photons carrying the information about fundamental processes at extreme conditions of the quark matter. The energy range of such photons extends from 0.4 GeV to 10 GeV for thermal radiation of Quark Gluon Plasma (QGP) and higher, up to hundreds GeV, for radiation occurring also in early collisions of the constituents. In the latter case the essential background is arising from the two-photon decay of  $^0$ -mesons, produced at the same energies as photons, due to the merge of decay photons into one shower in PHOS. Contribution of the photonic decay from heavier meson resonances ( $\rho$ ,  $\omega$ ,  $\eta$ , etc.) exists as well. Such photons provide a rather heavy background to direct photon production over the whole  $p_T$  range and they should be subtracted from the data. It leads to the necessity of identifying the PHOS showers as those produced by the photons or  $^0$ -mesons.

The straightforward way to discriminate the considered background from direct photons is to exploit a powerful reconstruction program tuned especially for the given PHOS structure and able to resolve the main problem of the "direct" photon selection (say, by the maximum likelihood method), and correspondingly, to find the real number of the showers even in the overlapped clusters. To accomplish this task, a program should correctly take into account the shower profiles of photons and charged particles at different incident angles, as well as their fluctuations, the electronics noise, the threshold on registered signals (that increases the number of zero channels in the selected cluster), etc. In practice such a perfect program is often too complicated for fast realization with long tuning and commissioning and additionally needs essential computational resources. Therefore, real reconstruction programs are usually created in some simplification assumptions which results in the degradation of its discrimination power for direct photon selection. Such simplified programs are often based on the recognition of the shapes of the showers produced by different kinds of particles.

In this paper we apply the Artificial Neural Network (ANN) approach [7] for the direct photon identification in PHOS. The ANN-method has already recommended itself as a powerful tool in different applications of high energy physics, e.g. quark and gluon jet separation, b-quark identification, Higgs boson search, selection of the rare neutral meson decay modes violating C-parity, etc. [8-13].

The main peculiarity of our method is the use of the energy-profile tensor of a cluster, which components are calculated in its eigen-vector coordinate system, with the aims of the neural net training and the afterward event classification. Our calculations show essential recognition capacities of this procedure that were examined using a sample

of Monte-Carlo generated events simulating the isolating production of direct photons and  $\phi$ -mesons for the real ALICE set-up.

## 2 Application of neural network algorithm method

In the analysis of experimental data, a standard procedure of selecting signal events is based on various cuts of observed kinematics variables. A general case of such cuts corresponds to a particular set of functions, called feature functions or neurons. In general terms, neural networks are represented as a large number of interconnected functional units named nodes with a neuron in each of them. The data processing is organized in the most common, to-date, architecture called the Multilayer Perception (MLP). MLP incorporates one input layer through which the initial data (features) are injected, several hidden layers, and one output layer of neurons.

Output response  $O_i$  of the  $i$ -th neuron is obtained by the so called sigmoid function  $f(x) = \frac{1}{1 + e^{-x}}$  dependent on the weighted sum of all input signals  $S_j$  to this neuron:

$$O_i = f\left(\sum_j w_{ij} S_j + \theta_i\right); \quad (1)$$

where index  $j$  runs over all the inputs of the  $i$ -th node,  $w_{ij}$  and  $\theta_i$  are the weights and the correspondent thresholds optimizing the selecting power of the procedure. Function  $f$  is defined as

$$f(x) = \frac{1}{1 + \exp(-x)}; \quad (2)$$

The output layer, consisting of one node, provides a neural-net response  $S_{NN}$ , wedged between 0 and 1, and used to classify the events.

The use of the neural network is a two-step process, i.e. a learning stage followed by an application stage. During the learning phase using the Monte-Carlo simulation, we know about every event whether it is a background or a signal one. The optimal values of weights  $w_{ij}$  and thresholds  $\theta_i$ , (see (1)), for resolving the problem are determined by minimizing the functional  $L(w_{ij}; \theta_i)$

$$L(w_{ij}; \theta_i) = \frac{1}{2} \sum_{k=1}^{X^N} \left[ S_{learn}^{(k)} - S_{NN}^{(k)} \right]^2; \quad (3)$$

where index  $k$  runs over all  $N$  training events,  $S_{learn}^{(k)} = 0$  for the background and  $S_{learn}^{(k)} = 1$  for desired events,  $S_{NN}^{(k)}$  are the ANN response. The details of the whole minimization procedure can be found in [14]. And finally the quality of learning is tested with an independent sample of Monte-Carlo events.

### 2.1 Input variables for the ANN

Reconstruction programs for cellular electromagnetic calorimeters provide data as a set of clusters defined as a group of cells with a common edge. Every cluster is characterized by the amplitudes of signals from the cells and coordinates of the cluster cells on the detector plane. The total length of the data array for one cluster is  $3N_c$ , where  $N_c$  is a number of cells in the cluster. This array contains exhausting experimental information about the cluster but, however, it is not convenient for the aim of the ANN approach, at least due to the varying data length from event to event. To overcome the latter problem one can use only the limited number of major cluster cells (say, 3-3 around the cell with the maximal amplitude [15]), but it definitely leads to the uncontrolled information loss.

The essential part of our ANN-approach to  $\theta = 0$  selection is to choose such a fixed number of variables that carry, nevertheless, the principal part of information with its volume big enough to find a solution and which length is independent of the cluster size. First of all each cluster is characterized by a position of its center-of-gravity  $X_g$  as well as by the center of the cell with the maximal signal in the cluster  $X_m$ . Vector  $X_g$  is defined according to the standard formula

$$X_g = \sum_k x^{(k)} E_k = \sum_k E_k; \quad (4)$$

where index  $k$  runs over all cluster cells,  $x_1^{(k)}$  and  $x_2^{(k)}$  being the coordinates of the  $k$ -th cluster cell in an arbitrary coordinate system.

Then we introduce an energy-profile tensor  $Q_{ij}$  of a cluster (that can be also interpreted as a  $2 \times 2$  matrix) calculated in the local cluster coordinate system. There are two natural possibilities to set the origin of this coordinate system: either in the center of gravity  $X_g$  or in the center of the cell with the maximal signal in the cluster  $X_m$ . In our calculations we choose the latter option. After that  $Q_{ij}$  is defined as

$$Q_{ij} = \sum_k x_i^{(k)} x_j^{(k)} E_k; \quad i, j = 1; 2; \quad (5)$$

Here index  $k$  runs over all the cluster cells,  $x_1^{(k)}$  and  $x_2^{(k)}$  are coordinates of the  $k$ -th cluster cell, for definition, in non-dimensional units of the crystal transverse size, and  $E_k$  is the energy detected in this cell. Tensor (5) is a quadratic positive-definite form.

The introduced tensor (5) reflects the cluster energy profile which depends on the number of showers overlapped in one cluster, as well as on inclination of the photon incidence on the detector. To avoid the latter effect or, at any rate, to decrease it we have made (before calculating matrix  $Q_{ij}$ ) a compression of the cluster space relative to the origin of the local cluster coordinate system  $X_0 = (x_{10}; x_{20})$  along the vector directed from the geometrical center of the PHOS module to the point  $X_0$ . The compression coefficient has been defined as  $c = \cos \alpha$ , where  $\alpha$  is the angle between the perpendicular to the PHOS module surface and the photon propagation direction. The coordinate transformation due to the compression operation has been made according to the formula

$$x' = R(\alpha) E_c(\alpha) R(\alpha) x = X_0 + X_0'; \quad (6)$$

where  $x = (x_1; x_2)$  is the vector of coordinates of an arbitrary transferred point,  $R$  and  $E_c$  are the matrices of rotation and compression, respectively:

$$R(\alpha) = \begin{pmatrix} \cos \alpha & \sin \alpha \\ \sin \alpha & \cos \alpha \end{pmatrix}; \quad E_c = \begin{pmatrix} \cos \alpha & 0 \\ 0 & 1 \end{pmatrix} \quad (7)$$

and  $\alpha$  is the polar angle of the point  $X_0$  in the polar coordinate system with its origin in the geometrical center of the PHOS module.

One can calculate two eigen values  $\lambda_1$  and  $\lambda_2$  (ordered as  $\lambda_1 \geq \lambda_2$ ) of  $Q_{ij}$  and find the correspondent eigen vectors  $e_1$  and  $e_2$  (normalized to a unit), defining a new coordinate system, where  $Q_{ij}$  is reduced to the diagonal form. In this new system we also define moments  $M_{mn}$ :

$$M_{mn} = \sum_k (x_1^{(k)})^m (x_2^{(k)})^n E_k; \quad m, n = 0; 1; 2; \dots; \quad (8)$$

where index  $k$  runs over the cluster cells,  $x_1^{0(k)}$  and  $x_2^{0(k)}$  are the coordinates of the  $k$ -th cluster cell in the new coordinate system. Note that  $M_{20} = \beta_1$ ,  $M_{02} = \beta_2$ , and  $M_{00} = E = \sum_k E_k$  is the total cluster energy. Such important magnitudes as distance  $d$  between hits of two glued photons and their effective mass  $M_{\text{eff}}$  can also be expressed through  $M_{mn}$  (see addendum).

We would also like to point out an essential remark. Initially the experimental information was carried by signal amplitudes and cell coordinates, and now it is represented by the introduced moments  $M_{mn}$ . We shall construct from  $M_{mn}$  the input vector  $\vec{P}^{(in)}$  of event features for ANN. One additional angle variable, not directly expressed through the  $M_{mn}$ , can be added. This is angle  $\theta$  between the eigen vector  $e_1$  and vector  $\vec{X}_0$  directed from the geometrical center of the PHOS module to the cluster center

$$\theta = \arccos(\vec{e}_1; \vec{X}_0 = \vec{X}_0^j): \quad (9)$$

The use of this angle, together with the coordinates of the cluster center on the detector plane, significantly improves the quality of  $\pi^0$ -selection mainly in the peripheral region of the PHOS modules.

We have found that there are different sets of variables that allow to construct effective event feature vectors. They include the total detected cluster energy, the eigen values  $\beta_1$  and  $\beta_2$ , the moments  $M_{mn}$ , the estimation of the effective mass  $M_{\text{eff}}$  and distance  $d$  between  $\pi^0$ -hits expressed through  $M_{mn}$  (see formulas (A.4) and (A.5)), and the angle variable  $\theta$ . Coordinates of the cluster center  $\vec{X}_0$  relative to the center of the PHOS module can also be added, which increases the selection power of the method.

## 2.2 Strategy of the $\pi^0$ -selection

In this section the algorithm of the  $\pi^0$ -selection is discussed in detail. First of all we note, that at low energies there is a background from  $\pi^0$  decays producing two separated clusters in PHOS that can be taken into account by one of the statistical methods, based on a good resolution of PHOS for  $M_{\text{eff}}$ -effective masses in this case, which is demonstrated below in Fig.5b. The mentioned procedures can, for example, reject the  $\pi^0$ -contribution by calculating the masses of  $\pi^0$ -combinations and by comparing them with the  $\pi^0$ -mass. It is possible to reduce the number of such combinations at high occupancy of the detector by taking into account the characteristic angle of the decay cone for photons. These methods are beyond the scope of the current paper. Thus, further calculations were fulfilled following the assumption that this type of backgrounds had been eliminated correctly.

Besides, there are two other essential sources of the background due to  $\pi^0$ -decays, when only one cluster appears in PHOS. The first one results from the detector geometry, i.e. when one of the decay photons from  $\pi^0$  escapes detection in PHOS due to the limited acceptance, whereas the second photon hits PHOS and generates a single shower and therefore a single cluster. It provides actually indistinguishable from the direct photons sample of the background photons in the whole photon energy range. This background is essential at relatively small energies of neutral pions. To suppress the relative part  $u$  (close to one) of such a background, we demand that the cone with a specially defined total angle  $\theta(u)$  around the photon propagation should cross the detector plane inside of it. The angle  $\theta(u)$  can be easily estimated from the isotropy of  $\pi^0 \rightarrow \gamma\gamma$  decay in the meson rest frame after the Lorentz boost to the laboratory system

$$\theta(u) = \arctan \frac{m_0(1+u) \sqrt{1-u^2}}{2E(1+u)} + \arctan \frac{m_0(1-u) \sqrt{1-u^2}}{2E(1-u)}; \quad (10)$$

where  $E$  is the energy of the analyzed cluster,  $\beta$  is the  $\pi^0$ -meson velocity in units of the light speed. Note that minimal decay cone angle  $\theta_{min} = 2 \arccos(\beta)$  can be obtained from formula (10) at  $u = 0$ . In the case when both photons fly towards the detector direction we arrive at  $u < \beta$ . To apply the considered cut we take  $u = 0.95$ . This cut actually works at small energies, and mainly at the edges of the calorimeter, while at high energies practically all events pass it successfully.

The second background comes from the limited spatial resolution of PHOS, i.e. when the overlapping showers from two-photon decays of the high-energy pions form one cluster. This mechanism provides the major background for direct photons at high energies. Its suppression is mainly fulfilled by the ANN-algorithm. The step sequence runs as follows.

First we apply the procedure of the local peak number determination in a cluster. It classifies the cluster as that with two overlapping showers when two local peaks are observed above the electronic noise fluctuations. Such classification of clusters is a common algorithm in reconstruction programs for cellular detectors.

To decrease the background from the decays  $\pi^0 \rightarrow \gamma\gamma$ , when only one photon hits PHOS due to the limited aperture, we apply cut (10) with the use of  $\beta(u)$ . The remaining clusters with one peak passing this 2-stage preselection are analyzed by ANN. It was composed of three layers (see Fig. 1): input, hidden and output. The input layer consists

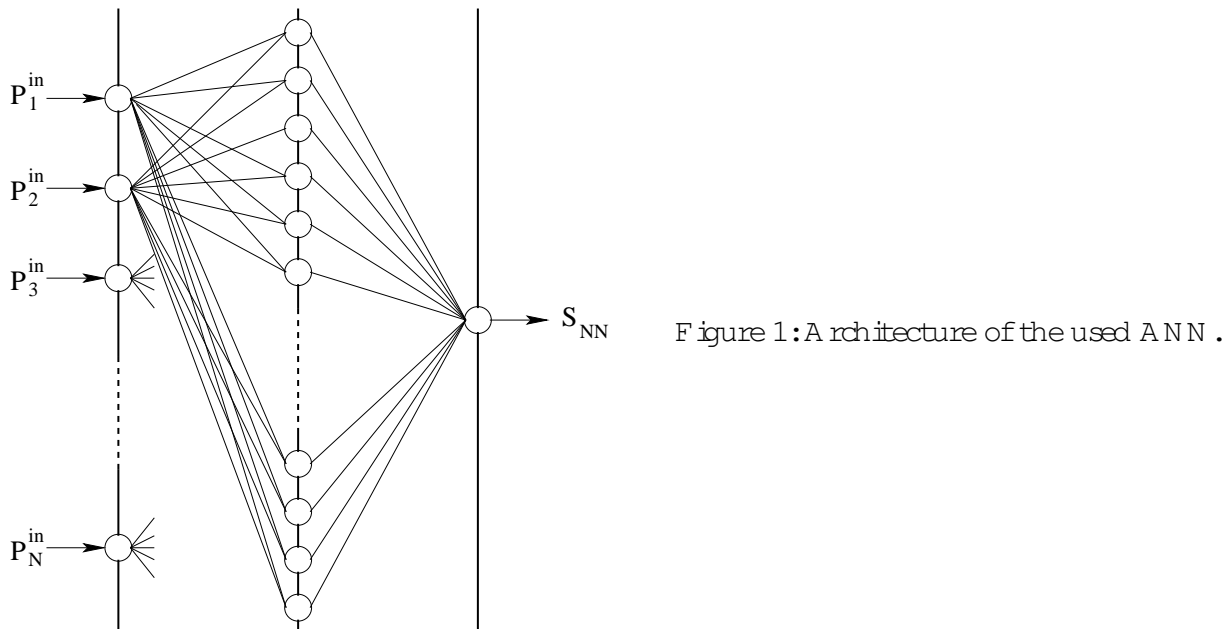


Figure 1: A architecture of the used ANN.

of  $N$  nodes, where  $N$  is the dimension of vector  $P^{(in)}$  representing the event features; the hidden layer is built of  $2N + 1$  nodes; and finally, the one-node output layer provides the neural-net response  $S_{NN} \in (0;1)$ .

The net was trained with two samples of events containing the desired signals (i.e. clusters from direct photons) and the background (i.e. clusters produced by the overlapped photons from decay  $\pi^0 \rightarrow \gamma\gamma$ ). Each sample consisted of 30,000 events (clusters) left after preselection. Upon training the net, we tested its efficiency on another statistically independent signal and background samples, each consisting of 30,000 events also left after the preselection.

### 3 Simulation of isolating photons and $\pi^0$ -mesons

The data taken for the analysis were simulated within the ALICE framework for the simulation, reconstruction and data analysis, alihroot v.3.06.02 [16]. Two samples

of events were generated, one sample containing one photon and another sample having one  $\pi^0$  per event. Photons and  $\pi^0$ 's were emitted from the interaction point with the uniformly distributed transverse momentum in the range of  $0 < p_T < 120$  GeV/c within the solid angle defined by the uniformly distributed azimuthal angle  $210 < \phi < 330$  and the polar angle  $80 < \theta < 100$ . The solid angle of the emitted particles was chosen to be a little larger than that of PHOS detector, to avoid various border effects. The decay of  $\pi^0$ 's was performed by the aliroot.

The real ALICE environment was taken into account during the particle tracking from the interaction point to PHOS. The following detectors and infrastructure modules which cover the PHOS aperture were installed: PIPE, ITS, TPC, TRD, FRAME, as shown in Fig. 2. This environment results in particle interactions with the media and the

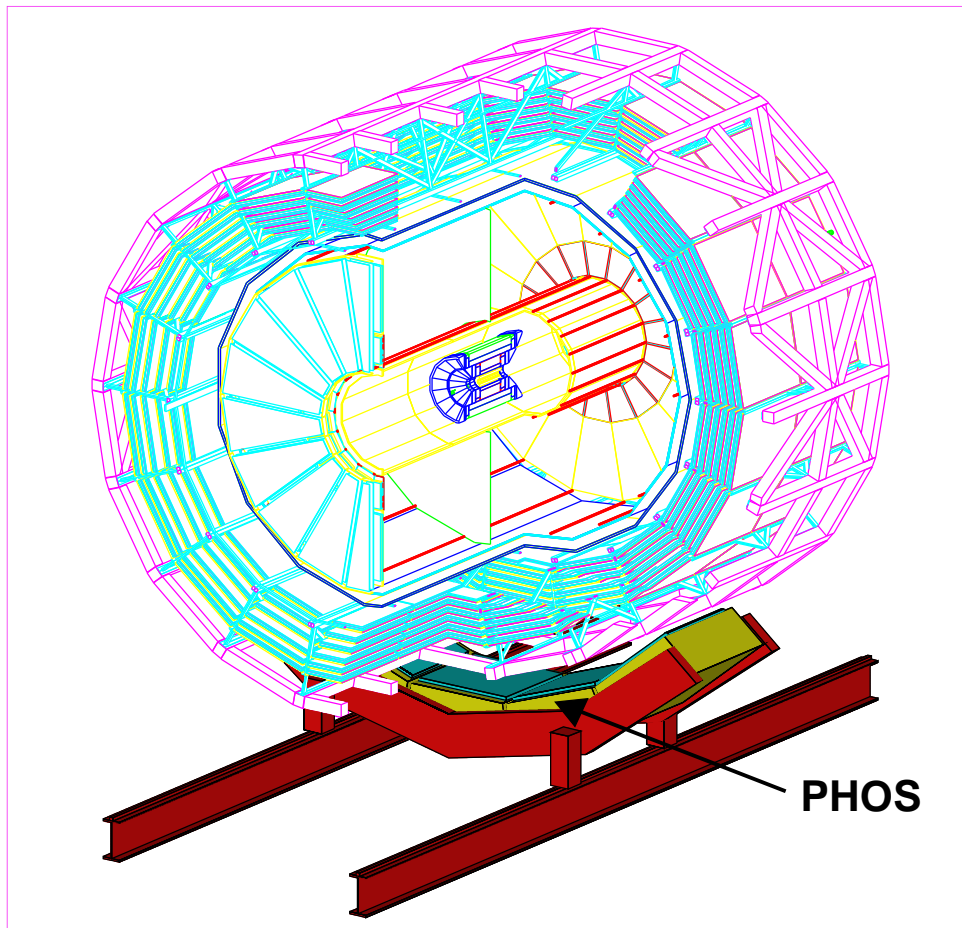


Figure 2: ALICE detector used for the simulation in aliroot.

production of secondary particles which deteriorate the response of the PHOS detector.

The response of the PHOS calorimeter was simulated by GEANT 3.21 [17], which was included into the aliroot package as a particle tracking and physics interaction tool. The showers developed by the particles passing through the calorimeter cells, gave the HITS which were the deposited energy of the shower in each cell. These HITS were digitized, i.e. the energy amplitude of the cell was measured by the two-channel ADC, and the integer signal of the ADC produced DIGITS. The noise with  $\text{noise} = 10$  MeV was applied to the DIGITS, after which the DIGITS were passed through the 50-MeV threshold cut. The remaining DIGITS with a common side were grouped into clusters. Only clusters with the total energy greater than 500 MeV were accepted.

The data that passed to the Neural Network analysis contained the following information. The event samples (photons or  $\pi^0$ 's) were identified by the file name. Events had a header which was characterized by the event number, the energy of the produced particle and the number of the found clusters. The event header was followed by the cluster data consisting of the cluster header with the cluster number and the number of cells in the cluster, and the cell information containing the list of cell positions in PHOS as well as the cell amplitudes.

#### 4 Results of the $\pi^0$ -selection

A analysis of the generated data shows that only 0.04% of direct photons are reconstructed as two-cluster events. The energies of the additional clusters are limited, they are practically not greater than 1.5 GeV.

Two-dimensional plots (Fig.3) of eigen values  $\lambda_1$  and  $\lambda_2$  versus energy E of  $\pi^0$  or  $\gamma$ , demonstrate the difference between the direct photons and the background that is used in the process of the ANN training. Fig.4 also shows one-dimensional distributions which demonstrate a rather well-expressed  $\pi^0$ -distinction.

Fig.5 shows comparative results of the calculations of effective masses  $M_{eff}$  for overlapped and separated clusters from  $\pi^0$ -decays and the same data from the sample of direct photons. For the overlapped clusters we use formula (A.5) expressing  $M_{eff}$  through the moments  $M_{mn}$ . In both cases for the overlapped and separated clusters from  $\pi^0$ -decays there are well observed peaks at the value of  $\pi^0$ -mass while application of the same formula (A.5) for direct photons gives a smoothly falling dependence with the growth of mass in the region of the  $\pi^0$ -meson. Smooth solid curves in the figure show the results of Gaussian fits of  $\pi^0$ -peaks. The average value and variation for the separated clusters are equal to 133 MeV and 6.8 MeV, respectively.

The main results of this article concerning the quality of the ANN training for the  $\pi^0$ -discrimination are presented in Fig. 6 for one of the possible feature event vectors, selected as  $(E; \lambda_1; \lambda_2; M_{30}; M_{04}; \dots)$ , where E is the measured cluster energy. The cut on the  $S_{NN}$  signal equal to 0.64. This figure shows the efficiency  $\epsilon(\gamma; \pi^0)$  of true photon identification as a photon, misidentification  $\epsilon(\pi^0; \gamma)$  of  $\pi^0$ -meson as a photon in the range of generated energies of photons and  $\pi^0$ -mesons from 3 GeV to 120 GeV, and the coefficient of background suppression relatively to direct photons  $\epsilon(\pi^0; \gamma) = \epsilon(\gamma; \pi^0)$ . One can see that the probability  $\epsilon(\pi^0; \gamma)$  of misidentification of a neutral pion as a photon is on the level of a few percent in the energy range of 3–120 GeV with relatively high efficiency of the true photon identification. The rise of the  $\pi^0$  misidentification probability at energies below 25 GeV is caused by the  $\pi^0 \rightarrow \gamma\gamma$  decays with one photon outside PHOS, whereas the decrease of the true photon identification efficiency at the energies below 15 GeV is the result of the true photon cut decreasing the background from these decays of  $\pi^0$ 's with only one photon inside PHOS.

We compare our results with the data of work [18] where the coefficient  $\epsilon(\gamma; \pi^0)$  was estimated for the STAR experiment as 0.15 at 20 GeV and 0.45 at 40 GeV at fixed  $\epsilon(\pi^0; \gamma) = 0.8$ . The efficiency of the  $\pi^0$ -recognition was also calculated within the neural network approach for the CMS experiment in note [15]. The obtained values  $\epsilon(\pi^0; \gamma)$  varied from 0.25 to 0.55 at  $E = 20$  GeV and from 0.40 to 0.55 at  $E = 100$  GeV, dependent on the rapidity range, while the efficiency of the single photon recognition was kept at 91%.



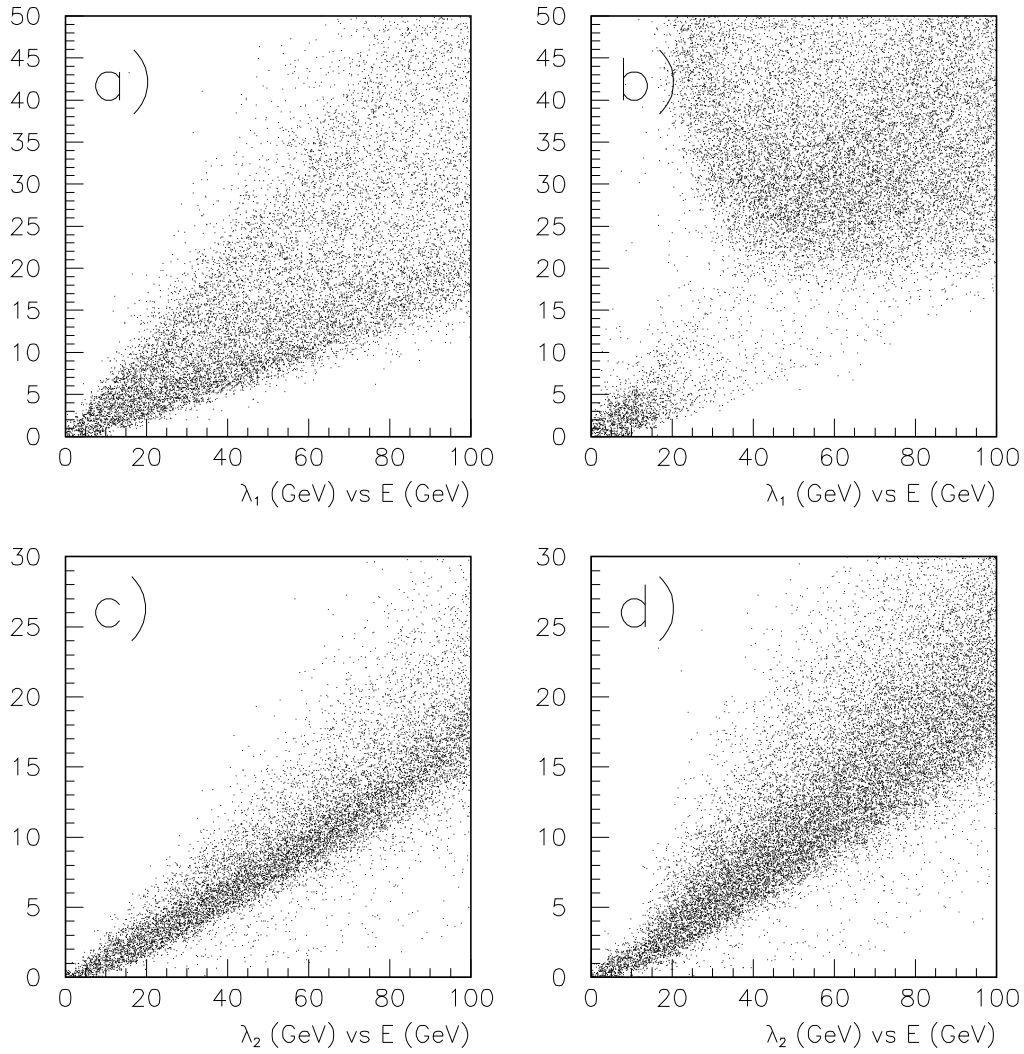


Figure 3: Two-dimensional plots of  $\lambda_1$  (a), (b) and  $\lambda_2$  (c), (d) vs energy, (a) and (c) are direct photons, (b) and (d) are the background.

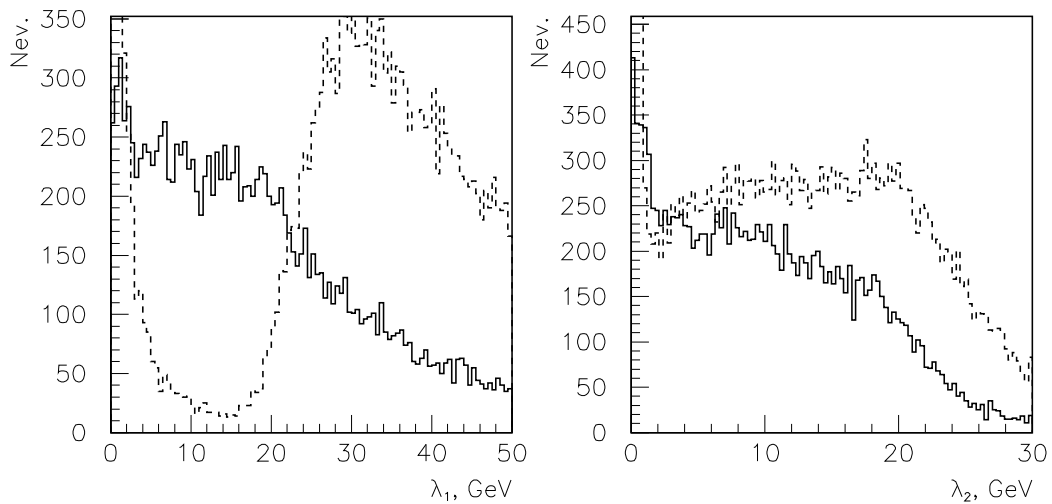


Figure 4:  $\lambda_1$ - and  $\lambda_2$  distributions for direct photons (solid lines) and background (dotted lines).

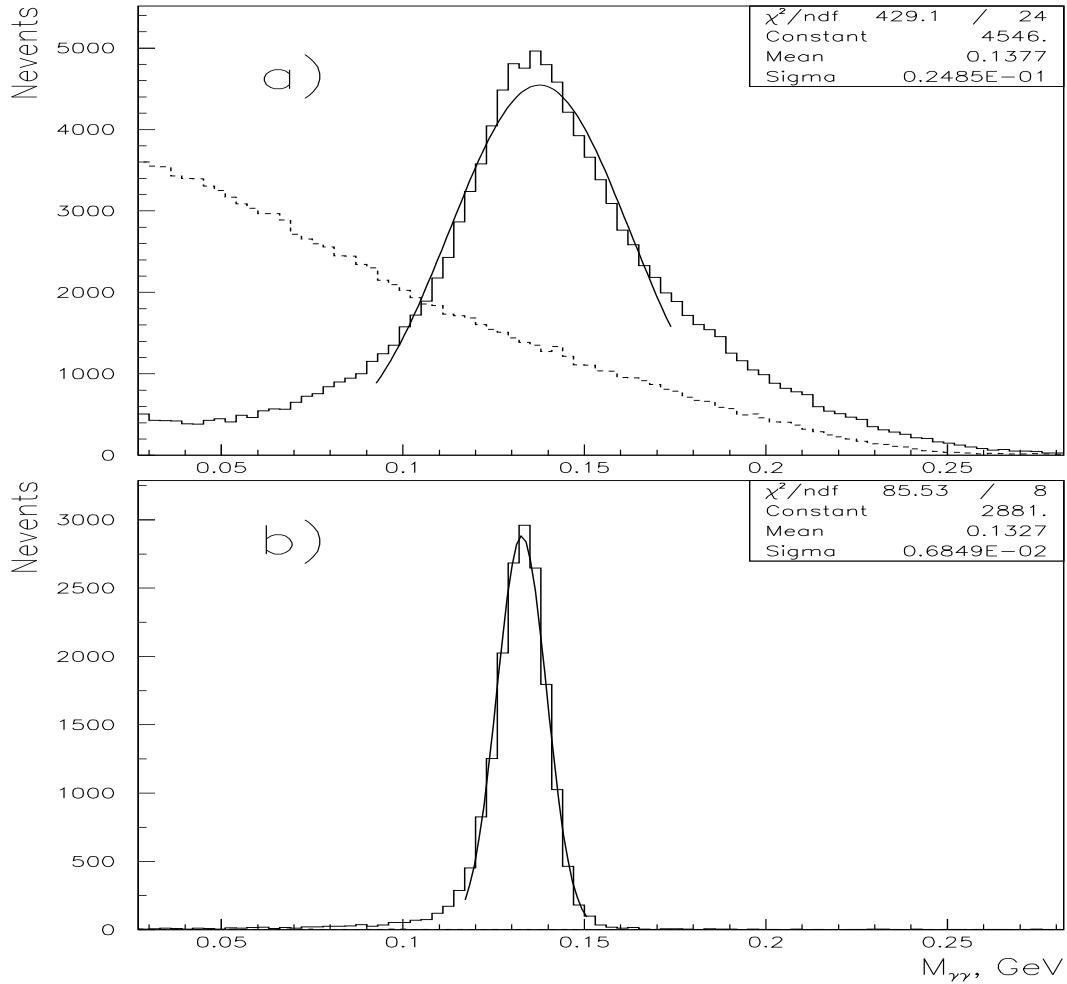


Figure 5: a) Distribution illustrating the results of calculating effective masses with formula (A.5) for overlapped clusters from the neutral pion decays (solid lines) and the same data for the sample of direct photons (dotted lines). b) Distribution of effective masses for the divided clusters from  $\pi_0$  decays. A mistaken contribution from the prompt photon due to the splitting of clusters under treatment is negligible on the level of unity events in the  $\pi_0$ -region. Smooth solid curves show the Gaussian fit with the average value of 133 MeV and the variation of 6.8 MeV.

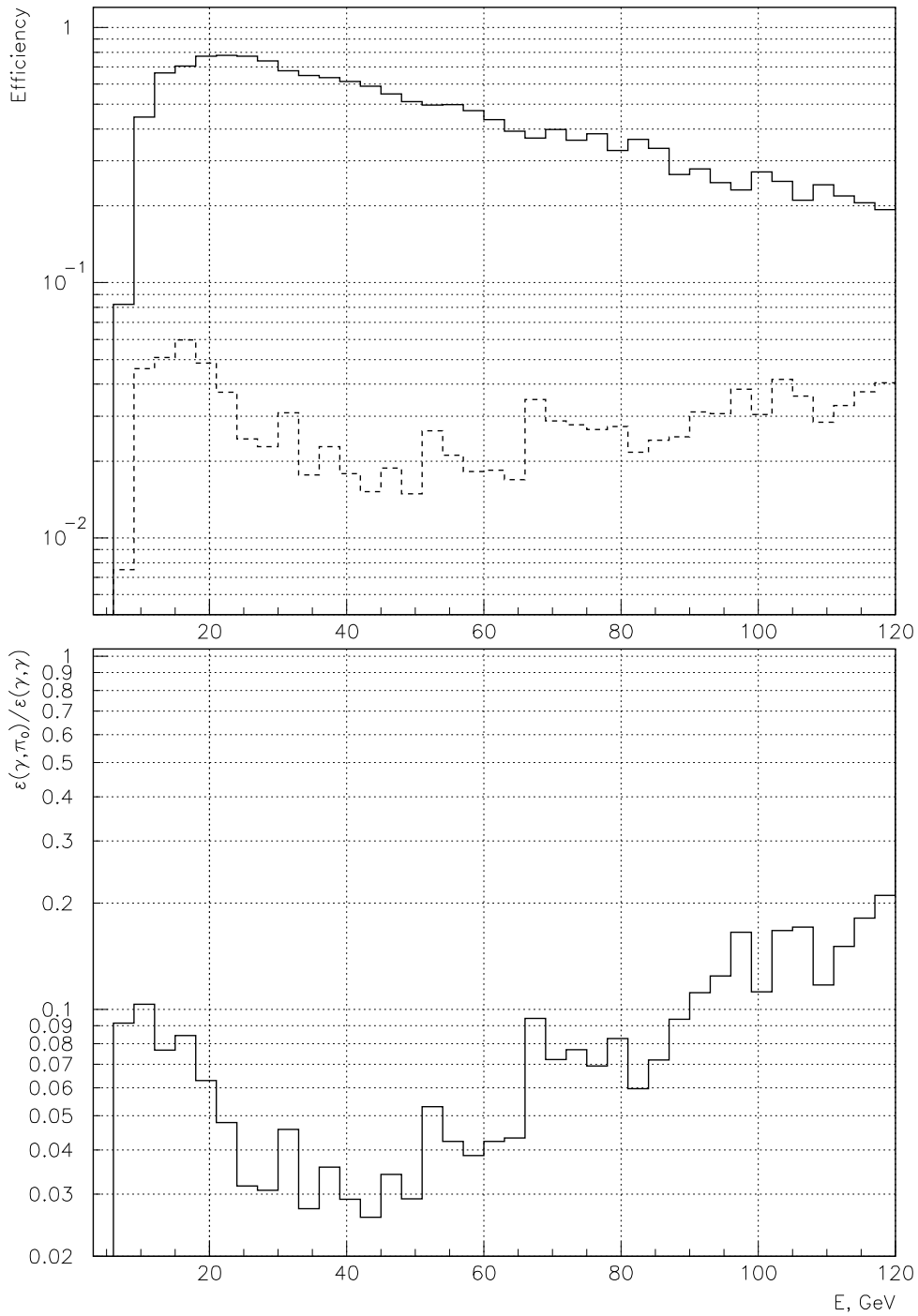


Figure 6: Efficiency  $\varepsilon(\gamma; \gamma)$  of true photon identification as a photon (solid lines), misidentification  $\varepsilon(\gamma; \pi^0)$  of  $\pi^0$ -meson as a photon (dotted lines), and the coefficient of the background suppression  $\varepsilon(\gamma; \pi^0) = \varepsilon(\gamma; \gamma)$  as a functions of  $E$ . The vector of event features is  $(E; i_1; i_2; M_{30}; M_{04}; \dots)$ .

## 5 Conclusion

In this paper a neural network method is developed to separate the direct photons from the neutral pion background in the PHOS spectrometer of the ALICE experiment. The proposed algorithm is based on the analysis of the energy-prole tensor of the cluster calculated in its eigen vector coordinate system. The proposed method allows to construct effective event feature vectors consisting of a limited number of variables carrying enough information to train the neural network for the goals of  $\pi^0$  separation. This method has been applied for Monte-Carlo events in PHOS. It has been found that the probability of misidentification of a neutral pion as a photon is on the level of a few percent in the pion energy range of 3–120 GeV with the relatively high efficiency of the correct photon identification as an isolated photon in the same energy range.

## References

- [1] ALICE Collaboration, Technical Proposal, CERN/LHCC/95-71, Geneva, 1995.
- [2] ALICE Collaboration, Technical Design Report PHOS, CERN/LHCC 99-4, ALICE TDR 2, Geneva,
- [3] ALICE Collaboration, Technical Design Report ITS, CERN/LHCC 99-12, ALICE TDR 4, Geneva, 18 June 1999.
- [4] ALICE Collaboration, Technical Design Report TPC, CERN/LHCC 2000-001, ALICE TDR 7, Geneva, 2000.
- [5] A M Blick, M Yu Bogolyubsky, A Di Mauro et al., Charged Particle Veto Detector with Open Geometry for the Spectrometer PHOS, ALICE Collaboration, Internal Note ALICE/PHOS 2000-21, 4 September 2000.
- [6] G Martinez, X Camard, H Delagrange et al., ALICE internal note ALICE-INT-2001-37.
- [7] L Lonnblad, C Peterson and T Rognvalson, Computer Physics Communication, 70, 1992; C Peterson, T Rognvalson and L Lonnblad, Preprint, LU-93-29, 1993; C Peterson, T Rognvalson and L Lonnblad, Preprint CERN-TH.7315/94, Geneva, 1994.
- [8] L Lonnblad, C Peterson and T Rognvalson, Phys. Rev. Lett. 65, 1321 (1990).
- [9] C Peterson, L Lonnblad, C Peterson and T Rognvalson, Nucl. Phys. B 349, 675 (1991).
- [10] P Bhat, L Lonnblad, K Meir and K Sugano, Proc. of the 1990 DPF Summer Study in High Energy Physics, Colorado, 1990.
- [11] I Scabai, F Czakó and Z Fodor, ITP Budapest report 477 (1990).
- [12] T Maggipinto, G Nardulli, S Dusini et al., Preprint BARI-TH/268-97, Bari, 1997.
- [13] A A Aseev, M Yu Bogolyubsky, V A Viktorov et al., Preprint IHEP 2002-3, Protvino, 2002.
- [14] C David et al., Phys. Rev. C 51 (1995) 1453.
- [15] E Reid and H F Health, CMS NOTE 2000/063, Geneva, 2000.
- [16] ALICE Offline Project. <http://AliSoft.cern.ch/offline/>.
- [17] GEANT, detector description and simulation tool. CERN program library long writeup W 5013.
- [18] N G Minaev, Preprint IHEP 94-142, Protvino, 1994.
- [19] S I Bitjukov, S A Sadovsky, V K Semenov and V V Smirnova, Preprint IHEP, 81-45, Serpukhov, 1981.

Addendum .

Calculation of effective mass through moments  $M_{mn}$

Kinematics formulae can be applied to estimate the effective mass  $M$  in the case of the divided clusters on the base of the measured energies of photons and the angle between their momenta. The problem is more complicated for the overlapped clusters. Here we follow paper [19] to express the mass  $M$  in terms of the above introduced moments (8) under assumption that the shower profile for an isolated photon possesses an azimuthal symmetry with respect to the point of hit. This leads to the following properties of the own moments  $M_{mn}$  (i.e. moments relative to the point of hit) for the isolated showers:  $M_{m0} = M_{0m}$  and  $M_{mk} = 0$  for odd  $k$ . The incidence inclination violates the azimuthal symmetry, but we restore it by the mentioned compression of the cluster space (6).

Due to the principle of energy additivity in the case of the overlapped showers the summary cluster energy density  $F(E_1; E_2; x_1; x_2)$  can be expressed in the eigen vector coordinate system of the cluster as follows:

$$F(E_1; E_2; x_1; x_2) = E_1 f(x_1 - x_{10}; x_2) + E_2 f(x_1 - x_{20}; x_2); \quad (A.1)$$

where  $E_1, E_2$  are the individual energies of showers,  $x_1$  and  $x_2$  are the coordinates of an arbitrary point in the cluster space,  $x_{10}$  and  $x_{20}$  are the coordinates of photon hits along the eigen vector  $e_1$ , and  $f(x_1; x_2)$  is the single photon shower profile. After that one can easily obtain from (8)

$$M_{ln} = \sum_{i=0}^{X^1} C_1^i [E_1 x_{10}^{1-i} m_{in} + E_2 x_{20}^{1-i} m_{in}]; \quad (A.2)$$

where a non-zero contribution gives only terms with even  $i$ ;  $C_1^i = 1/i!(1-i)!$  are binomial coefficients,  $m_{in}$  are normalized own moments  $m_{in} = M_{in}/M_{00}$  of a single photon shower. Taking into account the above mentioned azimuthal symmetry of single photon showers, we obtain the following set of equations for the determination of energies and coordinates of individual showers  $E_1, E_2, x_{10}, x_{20}$ :

$$\begin{aligned} \sum_{i=0}^8 E_1 + E_2 &= M_{00} \\ \sum_{i=0}^8 E_1 x_{10} + E_2 x_{20} &= M_{10} \\ \sum_{i=0}^8 E_1 x_{10}^2 + E_2 x_{20}^2 &= M_{20} \quad M_{02} \\ \sum_{i=0}^8 E_1 x_{10}^3 + E_2 x_{20}^3 &= M_{30} \quad 3M_{12} \end{aligned} \quad (A.3)$$

The solution is:

$$\begin{aligned} X &= \frac{M_{30} - 3M_{12} - M_{10}(M_{20} - M_{02}) - M_{00}}{M_{20} - M_{02} - M_{10}^2 - M_{00}} \\ d^2 &= X^2 - 4(XM_{10} - M_{20} + M_{02}) - M_{00} \\ &= (2M_{10} - XM_{00}) - d \\ E &= M_{00}; \end{aligned} \quad (A.4)$$

where  $X = x_{20} + x_{10}$ ,  $d = x_{20} - x_{10}$ ,  $\theta = E_2 / E_1$  and  $E = E_2 + E_1$ . The variable  $d$  gives the estimation of distance between the hits of individual showers in the overlapped cluster. To calculate the effective mass one should also know the distance  $R$  from the interaction point to the cluster center to determine the decay angle between quanta, and thus we obtain

$$M^2 = 4E_1 E_2 \sin^2(\theta/2) = (E^2 - d^2) \frac{d^2}{d^2 + 4R^2}; \quad (A.5)$$